LETTER Communicated by David Hansel

The Effects of Spike Frequency Adaptation and Negative Feedback on the Synchronization of Neural Oscillators

Bard Ermentrout
Matthew Pascal
Department of Mathematics, University of Pittsburgh, Pittsburgh, PA 15260, U.S.A.

Boris Gutkin
Unite de Neurosciences Intégratives et Computationelles, INAF-CNRS-UPR2191, 91198 Gif-sur-Yvette, France

There are several different biophysical mechanisms for spike frequency adaptation observed in recordings from cortical neurons. The two most commonly used in modeling studies are a calcium-dependent potassium current I_{ahp} and a slow voltage-dependent potassium current, I_m. We show that both of these have strong effects on the synchronization properties of excitatorily coupled neurons. Furthermore, we show that the reasons for these effects are different. We show through an analysis of some standard models, that the M-current adaptation alters the mechanism for repetitive firing, while the afterhyperpolarization adaptation works via shunting the incoming synapses. This latter mechanism applies with a network that has recurrent inhibition. The shunting behavior is captured in a simple two-variable reduced model that arises near certain types of bifurcations. A one-dimensional map is derived from the simplified model.

1 Introduction

Synchronous cortical rhythms are thought to be relevant to a number of higher cognitive processes and have been associated with selective attention and the binding problem (Gray, Engel, Konig, & Singer, 1992; Traub, Jefferys, & Whittington, 1999). Connections between different areas and cortical columns are mediated by excitatory interactions. It has previously been established that excitatory connections between neuron models that spike with no adaptation do not readily synchronize and in fact often fire in antiphase (van Vreeswijk, Abbott, & Ermentrout, 1994; Hansel, Mato, & Meunier, 1995). The reason for this is a consequence of the mechanism by which model cortical neurons make the transition from rest to repetitive firing. Ermentrout (1996) showed that if the transition to repetitive firing is through a saddle node on a circle bifurcation, then excitatory coupling will not generally lead to synchronous activity. Most models for fast spiking neurons have this property and thus will not tend to synchronize when

coupled with excitation. In this article, we define synchrony to mean a zero phase lag when two identical neurons are identically coupled. This is a mathematical idealization but allows us to be precise when we describe the locking behavior of coupled oscillators.

Cortical excitatory neurons are not generally "fast spiking." Rather, they are so-called regular spiking neurons and have spike frequency adaptation (McCormick, Connors, Lighthall, & Prince, 1985). In an earlier paper, Crook, Ermentrout, and Bower (1998) showed that the addition of spike frequency adaptation to cortical models enabled such models to synchronize stably with mutual excitation. The analysis in that article concerned a specific multicompartment pyramidal cell model and was strictly numerical. In this article, we systematically explore the role of adaptation in enhancing the synchronization properties of cortical neurons by studying the dynamics in the presence of adaptation and how this alters the response of the neural oscillation to inputs. We also show that the presence of recurrent inhibitory feedback works in the same way. Finally, we describe a "canonical" model that is valid near the onset of repetitive firing if the adaptation is sufficiently slow.

We first discuss two different types of adaptation: the calcium-dependent potassium current, I_{ahp} (afterhyperpolarization [AHP] current), and the muscarinic slow voltage-dependent potassium current, I_m (M current). We numerically show how they affect the synchronization of a model pair of cells. We then turn to an analysis of why this happens. We find that the M-current destabilizes the rest state through a Hopf bifurcation, which gives birth to a large-amplitude, stable, periodic solution. This has consequences for the phase-response curve (PRC), inducing a negative region that stabilizes synchrony. The AHP current acts in a more subtle manner and stabilizes by making the neuron insensitive to inputs that occur shortly after a spike (flattening the PRC) and sensitizing the neuron to inputs that come right before a spike (steepening the PRC). A similar effect occurs when the excitatory neuron is part of a network that contains inhibitory neurons as well. We finally show that this effect is captured in the canonical model.

2 Adaptation, Inhibition, and Negative Feedback

In many models of cortical neurons, there are two basic flavors of spike frequency adaptation: I_m, which is a slow voltage-dependent potassium current, and I_{ahp}, which is a calcium-dependent potassium current. Due to the slow kinetics of intracellular calcium accumulation, I_{ahp} can be quite slow. In typical models (see the appendix for some detailed equations), I_{ahp} is modeled by adding an L-type calcium current to the equations in addition to the spiking current. The L-type current has a fairly high threshold and a steep activation curve, and is generated only when the neuron produces a spike. Thus, I_{ahp} is turned on only if the neuron actually fires a spike. In contrast, for several models of I_m, there is a finite amount of the current present at rest in the neuron. The key qualitative (and quantitative) difference between

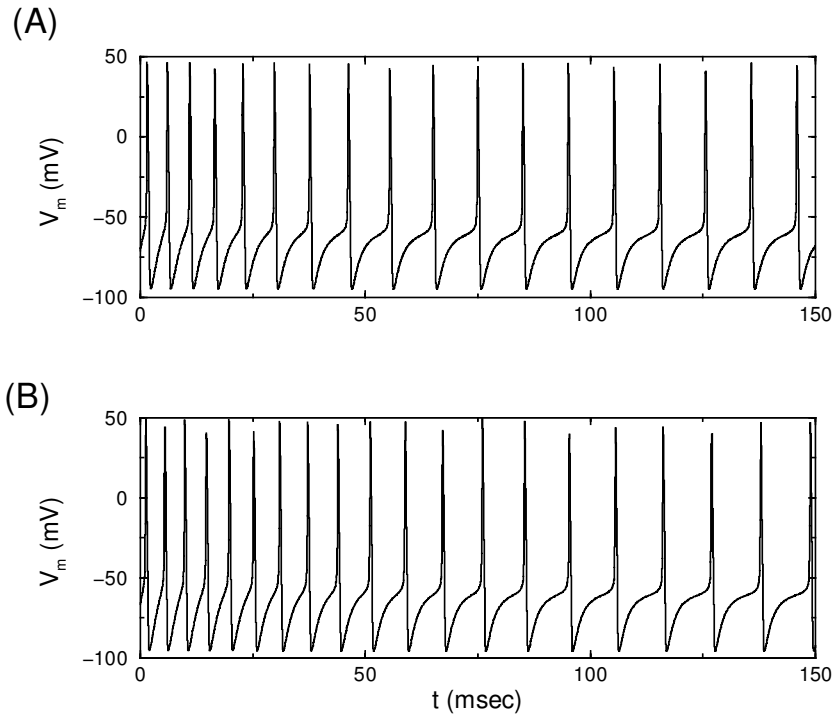

Figure 1: Spike frequency adaptation in the Traub model. (A) $g_m = 1$. (B) $g_{AHP} = 1$.

these two currents lies in their effective voltage dependence: the M current is less sharp and has a lower effective threshold, while the AHP current is sharper and has a higher effective threshold. Thus, more properly, we distinguish between low-threshold broad adaptation (exemplified by the M current) and high-threshold sharp adaptation (exemplified by the AHP current). In the appendix, we describe the conductance-based models used in this article; they are adapted from Traub and Miles (1991).

In Figure 1 we illustrate the two types of adaptation. In each case the injected current goes from 0 to 15 in a step. The initial firing rate slows to a steady-state firing rate. Note that the calcium-mediated adaptation takes slightly longer to reach a steady state.

Figure 2 shows the effects of spike frequency adaptation on a network of five globally coupled neurons. We plot the sum of the synaptic gates,

$$\mathrm{EEG}(t) = \sum_{j=1}^{5} s_j(t),$$

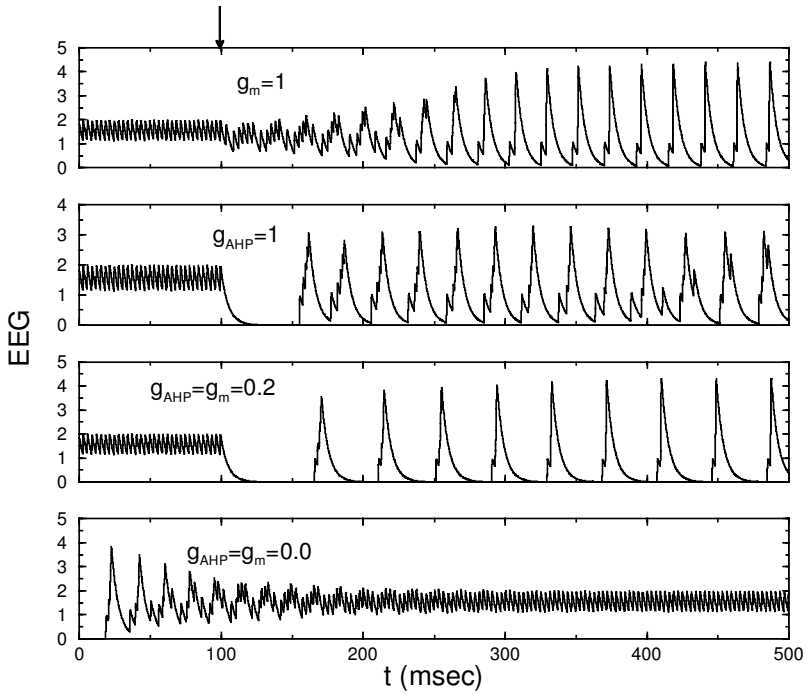

Figure 2: Effects of adaptation on the synchronization of a network of five synaptically coupled neurons. The total synaptic conductance felt by each neuron is plotted, $\sum_{j=1}^{5} s_j(t)$. In the first three panels, the initial 100 milliseconds show the behavior when there is no adaptation. The five cells all fire out of phase with each other. In the top panel, at $t = 100$ (arrow), the applied current is increased from $I = 0.6$ to $I = 6.0$ and $g_m = 1$. In the second panel, $I = 8.5$, $g_{AHP} = 1$, and in the third panel, $I = 2.5$, $g_m = 0.2$, $g_{AHP} = 0.2$. In the last panel, initial data are started very close to synchrony, and all adaptation is removed.

as this is a good measure of the total local current. With no adaptation, five identical all-to-all coupled neurons always go into the splay-phase state (one in which their phases are uniformly distributed). Adding adaptation in the form of the AHP or the M current (and increasing the applied current so that the uncoupled period remains the same) causes the five cells to synchronize or nearly synchronize. Starting from the nearly synchronous state, removing the adaptation, and reducing the applied current rapidly sends the network back into the desynchronized state. This synchronization is not particularly sensitive to noise and is robust to heterogeneities. (In the presence of heterogeneities, perfect synchrony with no timing differences is obviously impossible.)

Recurrent inhibition is in many ways like high-threshold adaptation. When the excitatory cell fires, it is sufficient to produce an action potential on a local inhibitory interneuron. This inhibitory neuron acts directly on the excitatory neuron and lowers the spontaneous firing rate. Thus, the presence of a local inhibitory interneuron can lower the firing rate of an excitatory neuron while at the same time having no effect on the stability and existence of the rest state. We have shown (Ermentrout & Kopell, 1998; Kopell, Ermentrout, Whittington, & Traub, 2000) that excitatory-inhibitory pairs are very good at producing synchronous behavior when the connections between such pairs are mediated by long excitatory-to-inhibitory connections. Below, we show that the presence of a feedback inhibitory neuron acts on the PRC curve of the excitatory neuron in the same way as high-threshold adaptation. Thus, excitatory-excitatory connections can produce synchronous or nearly synchronous activity. Figure 3 shows how the presence of recurrent inhibition can alter the synchronization properties of coupled excitatory neurons. Unlike the results cited above, there are only connections between the excitatory neurons.

2.1 Effect of Adaptation on the Bifurcation Diagram in a Model Cell. Despite its importance in shaping the responses of excitatory cortical neurons, there has been little systematic exploration of how the presence of adaptation affects the global behavior of a model neuron as currents are injected or other parameters are varied. Hansel et al. (1995), Ermentrout (1996), and Izhikevich (1999) have shown that the response of a neural oscillator depends crucially on the way in which the neuron makes the transition from rest to repetitive firing. There are two principal mechanisms by which a neuron makes the transition from rest to repetitive firing (Rinzel & Ermentrout, 1998). For Class I membranes, as the current increases, two equilibria (one stable and one unstable) coalesce and disappear. A large-amplitude oscillatory solution appears at this point with zero frequency. Ermentrout (1996) and later Izhikevich (1999) showed that for neurons with Class I membrane properties, the phase-response function is strictly positive. They also show that for a reasonable set of synaptic parameters, synchrony between excitatory neurons is unstable. For Class II, the onset of repetitive firing is through a subcritical Hopf bifurcation. The consequences are that the oscillations appear at a finite positive frequency, and there is often a regime of bistability between the stable fixed point and the oscillation. Hansel et al. (1995) numerically study the Hodgkin-Huxley model (which is Class II) and the Connor-Stevens model (which is Class I). For the former, they find that the phase-response curve has a substantial negative region, and this helps to stabilize synchrony between excitatory neurons. The best way to study parametric effects of adaptation on model neurons is to compute the bifurcation diagram as current is applied at different levels of adaptation. In this section, we show that the two distinct types of adaptation (M current and the AHP current, or low- and high-threshold adaptation,

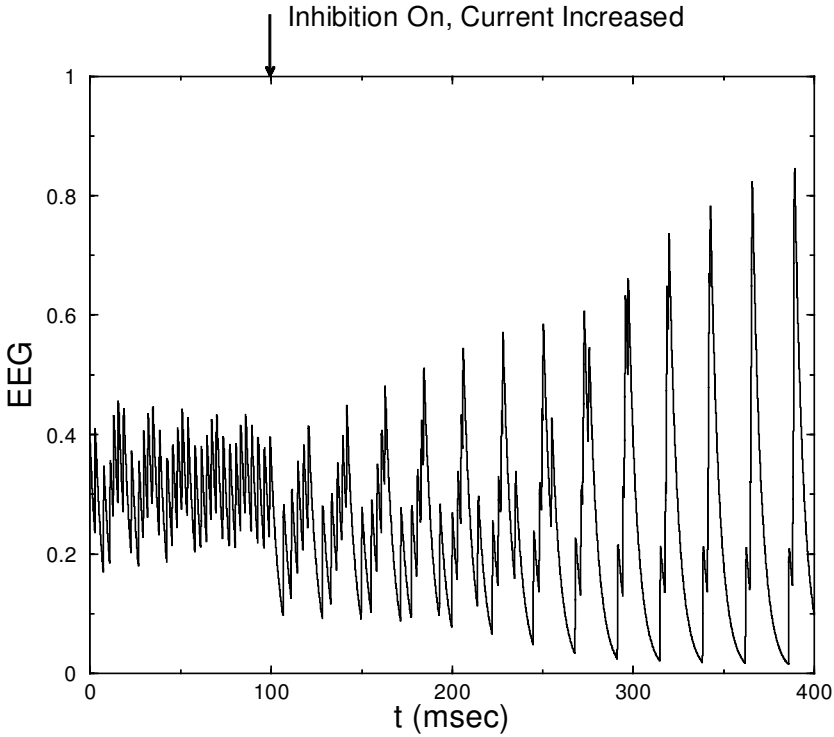

Figure 3: The introduction of local recurrent inhibition can also synchronize a group of coupled excitatory cells. The first 100 milliseconds show the behavior of the sum of the synaptic gates when there is no feedback inhibition and $I = 0.6$. Feedback inhibition is turned on and the current to the excitatory neurons is increased in order to maintain the same individual period ($g_{ie} = 1$, $I = 3.5$). The system approaches synchronous behavior. The network has five coupled "columns." Each column is a reciprocally coupled excitatory-inhibitory pair of cells. Coupling between columns is through all-to-all excitatory-excitatory synapses. Equations are found in the appendix.

respectively) have different qualitative effects on the stability properties of the rest state.

In order to perform this calculation, we have to choose a model neuron. Since we want a minimal set of currents in addition to the adaptation current, we have chosen a simple variant of Traub's model neuron (Traub & Miles, 1991) that contains only the currents required for spiking: transient sodium, the delayed rectifier, and a leak current. In addition, we have added an L-type calcium channel to implement the calcium-dependent potassium

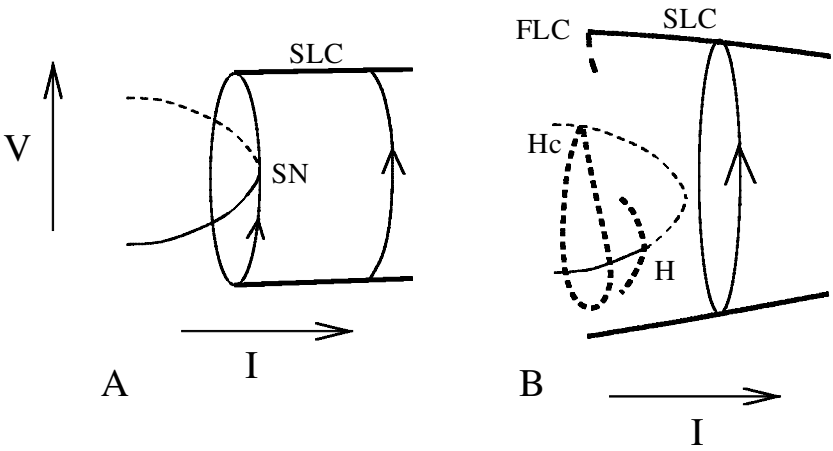

Figure 4: Cartoon of the bifurcation diagram for the conductance-based neuron model. The diagrams in the presence of g_{AHP} or recurrent inhibition are indistinguishable from the control case with no adaptation. (A) No adaptation. There is a curve of fixed points terminating at a saddle node (SN) point. Thin, solid lines are stable fixed points; dashed lines are unstable. For larger currents, there is a branch of stable periodic solutions that emerges from the saddle node with zero frequency (denoted SLC in the figure). (B) M current adaptation. The curve of fixed points remains, but the lower branch loses stability at a Hopf bifurcation (H). A branch of unstable periodic orbits (thick, dashed lines) emerges from the Hopf bifurcation and ends homoclinic to the unstable upper branch (Hc). A stable branch of limit cycles (SLC) terminates by colliding with an unstable branch at the point FLC.

current. The model is similar to one used by Wang (1998) in his study of spike adaptation and is described in the appendix.

In Figure 4, we sketch the bifurcation diagram of this model neuron as current is injected and there is no adaptation. (To distinguish the differences between the two diagrams more clearly, we offer only schematic pictures rather than the full numerically computed curves.) At low values of current, there is a stable fixed point representing the rest state. As the current increases, a saddle point and the stable node coalesce and disappear. The only stable behavior is repetitive firing, which appears precisely where the fixed points coalesce. This is typical behavior for Class I membranes. Since the AHP is essentially nonexistent at rest, it has no effect on the bifurcation of the equilibria. As the current increases, the critical value of the current at which the fixed point disappears via a saddle node is independent of the degree of adaptation. As with the case with no adaptation, a stable limit cycle appears for currents greater than the saddle node, and these emerge with zero frequency. Thus, adaptation mediated by a high-threshold calcium-

dependent potassium current has basically no effect on the equilibrium bifurcation curve. Furthermore, it does not change the nature of the branch of periodic solutions other than to lower their frequency. The same can be said for a network of one excitatory and one inhibitory neuron in which current is injected only into the excitatory cell. (Equations for this network are also given in the appendix.) As we will see below, however, high-threshold adaptation or recurrent inhibition has a dramatic effect on the response of the oscillation to perturbations.

In contrast to the high-threshold calcium-mediated adaptation or recurrent inhibition, the M current *does* have an effect on the bifurcation curve. Since it is nonzero at the resting potential, we expect that it will affect the onset of repetitive activity. Figure 4B demonstrates the effect on the rest state. First, the disappearance of fixed points occurs at a much larger current. The presence of a resting level of M current acts to delay the bifurcation by providing a nontrivial outward current. The other (and more important) effect of the M current is that it also causes the lower branch of fixed points to lose stability at a Hopf bifurcation. This bifurcation is subcritical, and the resulting unstable periodic orbit meets with the unstable fixed point at a homoclinic point. The large-amplitude stable branch of periodic solutions extends for currents beyond the Hopf bifurcation and disappears in a collision with a branch of unstable periodic solutions. There is a very small range of currents where there is a stable limit cycle coincident with a stable equilibrium point. Since the stable periodic orbit disappears at a finite nonzero frequency near a subcritical Hopf bifurcation, the adaptation changes the dynamics from Class I to Class II. As we will see, this has a major effect on the phase-response curve of the neuron.

Summarizing, the M current alters both the position of the bifurcation to periodic solutions and the nature of the bifurcation to repetitive firing. It converts a Class I neuron to a Class II. Neither the calcium-dependent potassium current (AHP current) nor the local inhibitory interneuron has an effect on the bifurcation of the equilibria and the emergence of repetitive activity at arbitrarily low frequencies. By lowering the threshold of the AHP current, we can make its effect like that of the M current. Similarly, by sharpening and raising the threshold of the M current, we can make it mimic the AHP current. From the point of view of the dynamics, the main difference between the two is that the M current is modeled as a low-threshold current while the AHP is a higher-threshold current.

3 The Weak Coupling Limit

Previous work on coupled neural oscillators (Ermentrout, 1996; Hansel et al., 1995) has shown that there are dramatic differences in the ability to synchronize according to whether the neuron is Class I (oscillations emerging from zero frequency) or Class II (oscillations emerging via a Hopf bifurcation). From the previous section, we see that low-threshold adaptation currents

alter the firing class of the neuron. Thus, we expect that the M current will have an effect on synchrony. The effects of the high-threshold adaptation or recurrent inhibition are not so obvious, although, as seen in Figures 2 and 3, both tend to stabilize synchrony. By analyzing the weak coupling limit, we can study this question precisely. We first briefly review the method for computing weak interactions between oscillators. We then apply the methods to the conductance-based model showing how adaptation affects the relevant curves.

3.1 Weak Coupling and the Phase-Response Curve. Suppose that two identical oscillators, X_1, X_2, are weakly coupled (that is, the coupling between them is sufficiently small so as not to distort the waveforms but rather alters only the timing). The general equations are:

$$X_1' = F(X_1) + \epsilon G_1(X_2, X_1) \quad X_2' = F(X_2) + \epsilon G_2(X_1, X_2). \tag{3.1}$$

We assume $0 < \epsilon \ll 1$ and $X_0' = F(X_0)$ has an asymptotically stable limit cycle, $X_0(t)$ with period T. Then it can be shown (see, e.g., Ermentrout & Kopell, 1984; Hoppensteadt & Izhikevich, 1997) that the solutions to equation 3.1 have the form

$$X_j(t) = X_0(\theta_j) + O(\epsilon),$$

where

$$\theta_j' = 1 + \epsilon H_j(\theta_k - \theta_j) + O(\epsilon^2) \quad j = 1, 2 \quad k \neq j$$

governs the evolution of the relative phases. The functions H_j are T periodic and can be readily computed for any given model. Before describing their computation, we briefly consider the above phase equations. Let $\phi = \theta_2 - \theta_1$ denote the phase difference between the two neurons. Then,

$$\frac{d\phi}{dt} = \epsilon(H_2(-\phi) - H_1(\phi)) = \epsilon d(\phi). \tag{3.2}$$

If $d(\phi) = 0$ for some ϕ, then the phase differences between the two oscillators is fixed, and there is a periodic solution to equation 3.1 with the phase difference $\phi \in [0, T)$ between the two oscillators. In particular, if $\phi = 0$, then the two oscillators fire synchronously. If $H_1 = H_2 \equiv H$, then $d(\phi) = -2H_{odd}(\phi)$ is proportional to the odd part of the interaction function, H. Any odd periodic function always has 0 and $T/2$ as roots. Thus, both the synchronous and the "antiphase" solution will exist for a pair of weakly coupled identical oscillators. A root $\bar{\phi}$ of $d(\phi)$ is a stable fixed point if $d'(\bar{\phi}) < 0$. For identical oscillators, this means $H'_{odd}(\bar{\phi}) > 0$. By simply looking at the odd part of the interaction function, we can pick out all the stable and unstable phase-locked solutions for two weakly coupled identical oscillators.

The computation of the interaction functions H_j can be done by successive changes of variables and then averaging. However, this is inefficient and is

not readily automated. We have shown (Ermentrout & Kopell, 1991) that this rigorous procedure is equivalent to the formal method of computing H in the manner of Kuramoto (1982):

$$H_j(\phi) = \frac{1}{T}\int_0^T X^*(t)\cdot G_j(X_0(t+\phi), X_0(t))\,dt. \tag{3.3}$$

The vector function $X^*(t)$ is the unique solution to the linearized adjoint equation:

$$\frac{dX^*(t)}{dt} = -[D_X F(X_0(t))]^T X^*(t) \quad X^*(t)\cdot\frac{dX_0(t)}{dt} = 1.$$

(By $[D_X F]^T$ we mean the transpose of the matrix of partial derivatives of F with respect to the variables, X.) The functions $X^*(t)$ are easily computed for any stable limit cycle (see Williams & Bowtell, 1997).

For equation 3.3, the effects of adaptation on the interactions between neural oscillations arise from two sources: changes in the coupling function and changes in the adjoint $X^*(t)$.

3.2 Specific Forms for Conductance-Based Models. In synaptically coupled one-compartment model neurons, coupling is only through the potential. That is, the coupling $G(\cdot,\cdot)$ is zero for all components except for the voltage. In particular,

$$G(X_2, X_1) = g_{syn}s_2(t)(V_{syn} - V_1(t)).$$

Here, $s_2(t)$ is the synaptic gating variable (often satisfying a differential equation or specified as a fixed function of the time since the presynaptic cell has fired). g_{syn} and V_{syn} are the maximal conductance and the reversal potential of the synapse. This means that for a pair of coupled neurons, the interaction function is simply

$$H(\phi) = g_{syn}\frac{1}{T}\int_0^T s_{pre}(t+\phi)V^*(t)(V_{syn} - V(t))\,dt, \tag{3.4}$$

where $V^*(t)$ is the voltage component of the adjoint. If we adjust input currents to the oscillators so that the period of oscillations is fixed, then the role of adaptation can be analyzed separately from the frequency effects. For a fixed-period oscillation, we do not expect adaptation to have much of an effect on the shape of the synaptic gating variable (since this just depends on the firing of an action potential); thus, all the changes in the function H that arise will be due to changes in the product:

$$V^*(t)(V_{syn} - V(t)).$$

For excitatory synapses, $V_{syn} = 0$ mV, so that the main effect of the term $(V_{syn} - V(t))$ is to multiply the adjoint $V^*(t)$ by an essentially positive function. ($V(t) > 0$ for only a very short fraction of the period.) Qualitatively, we see that if adaptation is to have an effect on the interaction, it will have to be through the adjoint $V^*(t)$.

The PRC is an experimentally measurable quantity (Reyes & Fetz, 1993a, 1993b) in which a brief pulse is applied to an oscillating neuron and the advance or delay of the next spike is computed. That is, suppose that T is the normal period of the cell. Let $\hat{T}(t)$ be the time of the next spike given that the stimulus has occurred at a time t after the last spike. Then the PRC, $P(t)$, is defined as the fraction change of the timing:

$$P(t) \equiv \frac{T - \hat{T}(t)}{T}.$$

Often only the timing advance or delay, $\Delta(t) = TP(t)$ is reported.

Hansel et al. (1995) have given a nice intuitive definition of the voltage component of the adjoint, $V^*(t)$. It is just the infinitesimal PRC. That is, let $P(t, a)$ be the PRC for a stimulus of amplitude a. Then $V^*(t) = \lim_{a \to 0} \Delta(t, a)/a$.

Since the period of the oscillation does not change with adaptation (as we compensate for this with additional injected current) and the synaptic time course does not change, the main effect of adaptation on the interaction between neural oscillators must be mediated through the PRC (approximated by the adjoint). Thus, we study the effects of adaptation on the PRCs and adjoints, $V^*(t)$, of conductance-based neural models.

3.3 Adjoints for Neural Models. Hansel et al. (1995) described adjoints for several different model neurons. In particular, they describe what they call Type I and Type II adjoints. Type I adjoints are strictly nonnegative; the effect of a depolarizing stimulus is either to do nothing or advance the phase. Model neurons like the Traub model above (without adaptation), the Connor model (Connor, Walter, & McKown, 1977), the Morris-Lecar model (Morris & Lecar, 1981), and the integrate-and-fire model are all examples of models with nonnegative PRCs. Ermentrout (1996) and Izhikevich (1999) showed that all neural models that have Class I membrane properties (this includes all the aforementioned models except the integrate-and-fire) are, near the onset of oscillations, equivalent to a simple canonical model that is described below. This model has a strictly positive PRC, $\Delta(t) = 2\arctan(\tan(t/2) + w) - t$, where w is the magnitude of the stimulus.

Type II (Hansel et al., 1995) adjoints are characterized by both positive and negative regions so that for stimuli shortly after the spike, the phase is delayed. The Hodgkin-Huxley model is of this type. Near a supercritical Hopf bifurcation, the adjoint has a form similar to $-\sin(2\pi t/T)$; thus, it is both positive and negative. The adjoint for certain classes of relaxation oscillators also has both positive and negative regimes (Izhikevich, 2000).

In addition to classifying the differences in adjoint types, Hansel et al. (1995) also numerically demonstrated that neurons with Type II adjoints can synchronize with excitatory coupling in contrast to neurons with Type I adjoints, which have difficulty synchronizing. This particular result suggests that one mechanism by which adaptation enables neurons to synchronize is to switch the adjoint from Type I to Type II. As we have already mentioned, the M current adaptation serves to change the saddle-node bifurcation (which leads to Type I adjoints) to a Hopf bifurcation (which results in Type II adjoints). Thus, the adaptation generated by the M current may work by changing the adjoint from a strictly positive one to one with a substantial negative regime after spiking.

3.4 The Variation of the Adjoint and the Interaction Function. In this section, we consider the model depicted in Figures 1 and 2 in the limit of weak coupling with different degrees of adaptation. In Figure 5 we show the effects of the M current adaptation on the adjoint, $V^*(t)$, in the left set of panels and the odd part of the interaction function in the right panel. In each panel, the degree of adaptation is shown, as well as the applied current. The current is chosen so that the period of the limit cycle is 25 msec. If we multiply $V^*(t)$ by $(V_{syn} - V(t))$, the shapes of the resulting curves are virtually unchanged except for the amplitude; thus, we show only the adjoints $V^*(t)$.

Figures 5 and 6 illustrate the effect of adaptation on the adjoint and the consequent effect on the interaction function for the Traub model (cf. Figures 1 and 2). Figure 7 shows a similar picture for the network with feedback inhibition. We first point out that with the M-current adaptation, synchrony becomes stable in the weak coupling limit since the slope of the odd part of the interaction function is positive. This is not the case for the high-threshold adaptation or for the network with recurrent inhibition; the best we can say is that there is a small phase difference between the two oscillators. We will see why this happens in the next section. The key feature responsible for making the phase difference between the pair of oscillators close to 0 is the flattening or negative region of the adjoint right after spiking. We can intuitively see why there is a tendency toward synchrony by looking at the different adjoints. Consider a pair of mutually coupled identical cells that are nearly synchronous. Cell 1 fires first, which advances cell 2. Cell 2 fires, and this advances cell 1. Thus, in one cycle, both cells are advanced. The phase difference between them will shrink if cell 2 is advanced more than cell 1. In the case of no adaptation, the advances are both positive and close in magnitude, so a more detailed analysis is required, and the width of the synapse plays a critical role. However, in the presence of adaptation, cell 1 is either not advanced at all (with the AHP current) or actually delayed (with the M current); thus, adaptation allows cell 2 to "catch up" to cell 1 in the sense that the phase lag between them shortens. This effect is quite strong and thus will not be as sensitive to the time course of the synapses.

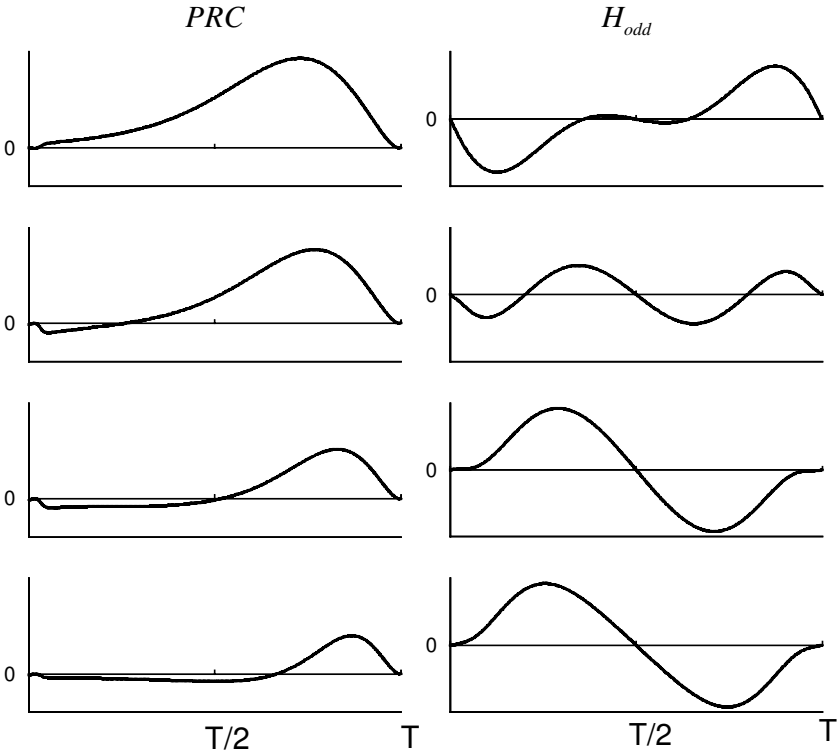

Figure 5: The adjoint and the odd part of the interaction function for the Traub model with M current (low threshold)–based adaptation. In each frame, sufficient current is injected into the model cell so that the frequency of oscillation is 40 Hz. Synapses are as in Figure 2. From top to bottom, $(g_m, I) = (0,0.922)$, $(0.2628,1.99)$, $(0.99,4.9)$, and $(2.477,10.3)$.

More formally, the following argument shows how changes in the adjoint can alter the stability of the synchronous state. Recall that the synchronous solution is stable if $H'_{odd}(0) > 0$, which implies $H'(0) > 0$. Thus, the condition for stable synchrony for two coupled, identical, synaptically coupled neurons is

$$H'(0) = \frac{1}{T}\int_0^T s'(t)(V_{syn} - V(t))V^*(t)\,dt > 0.$$

Consider the case with no adaptation. The adjoint is zero and then rises to some peak. Since $s'(t)$ is positive shortly after the spike and is negative thereafter, the integral is negative so that synchrony will be unstable. In the case of the low-threshold adaptation (M current), the adjoint is negative and grows in magnitude. Thus, the integral will be positive so that synchrony

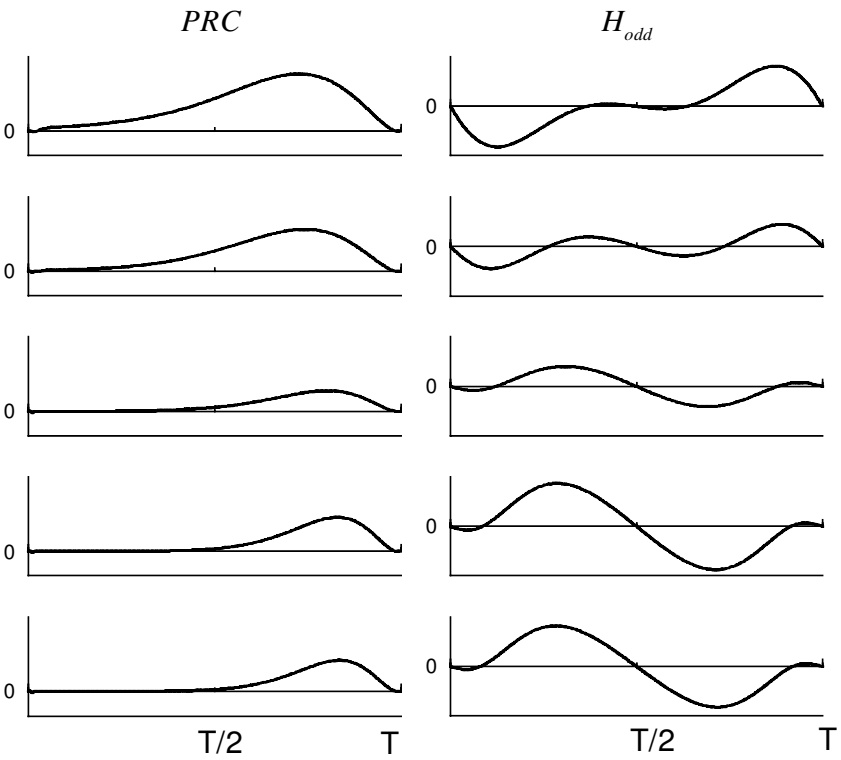

Figure 6: The adjoint and the odd part of the interaction function for the Traub model with AHP current (high threshold)–based adaptation. In each frame, sufficient current is injected into the model cell so that the frequency of oscillation is 40 Hz. Synapses are as in Figure 2. From top to bottom, (g_{AHP}, I) = (0,0.93),(0.262,3.06), (0.915,8.58), (1.368,12.455), and (1.48,13.43).

will be stable. For the case of high-threshold adaptation and recurrent inhibition, the situation is more subtle since the adjoint is nearly flat during the majority of time when the synapse is on. Numerical calculations are necessary. Indeed, as seen in Figures 6 and 7, synchrony remains unstable, but there is a stable, nearly synchronous solution.

We have discussed only the adjoints of oscillators with adaptation in this section. It is easy to compute the actual PRCs for these models by choosing an appropriate perturbing stimulus. Numerical calculations (not shown here) reveal that with a current stimulus with width 0.2 msec and magnitude 10, the PRC and the adjoint are indistinguishable up to a scale factor. The measured PRCs of cortical neurons resemble those of the Traub model with an AHP-type (or high-threshold) adaptation. In Figure 8 we show the

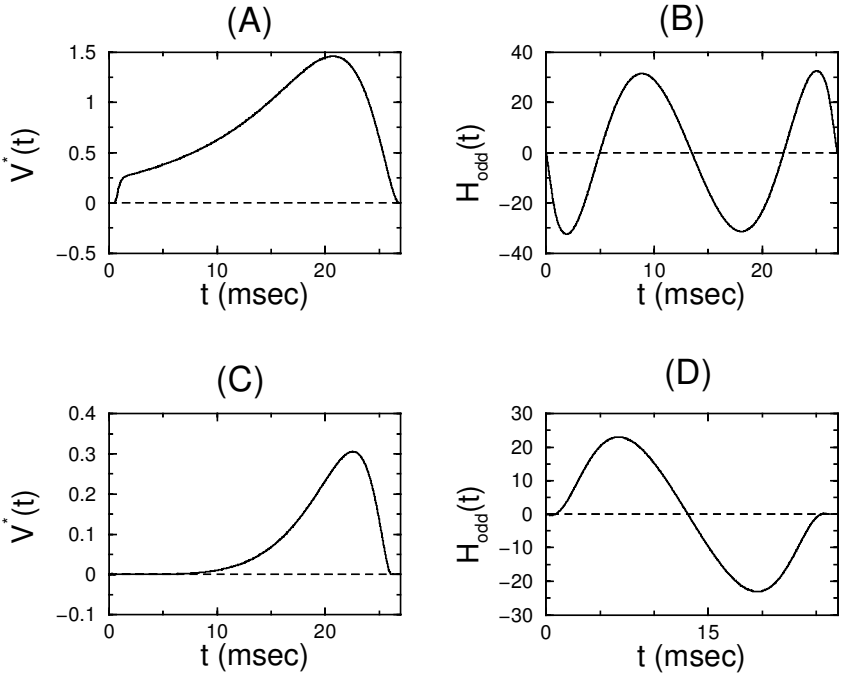

Figure 7: Effects of a local inhibitory interneuron on the adjoint and the interaction function. (A, B) Adjoint and H_{odd}, respectively, for the isolated excitatory neuron. Synchrony is unstable. (C, D) The same functions are shown, respectively, for an excitatory and an inhibitory circuit. The inhibition flattens the the response right after the spike. The resulting H_{odd} shows that synchrony is nearly stable.

experimentally determined PRC (Reyes & Fetz, 1993a) and an adjoint from the Traub model. It is difficult to tell whether there is a statistically significant negative region, so that one could possibly fit this with the M-current adaptation model.

Adaptation appears to encourage synchrony by either causing the neuron to ignore inputs shortly after it has spiked or to delay the onset of the next spike by producing a negative region in the PRC.

4 The Behavior Near the Bifurcation: A "Canonical Model"

In previous work (Ermentrout, 1996) we have shown that many models for spiking are Class I. That is, as the current increases, the model goes from rest to repetitive firing via a saddle node on a circle. Locally, a saddle-node

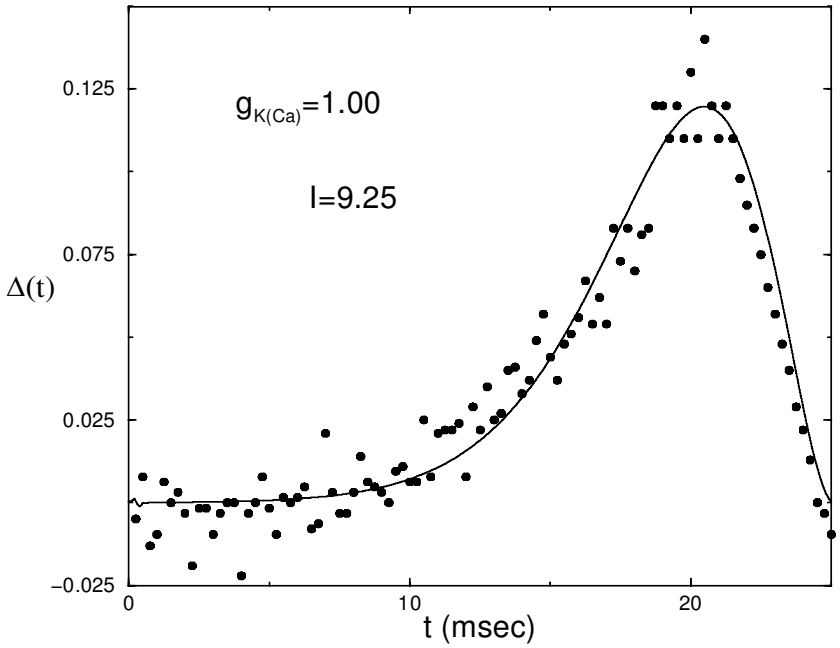

Figure 8: The PRC from a cortical neuron (see Reyes and Fetz, 1993b, and the PRC from the model in Figure 1 with a choice for g_{AHP} and I that closely matches the data. (Data supplied by A. Reyes.)

bifurcation has the form

$$x' = I + x^2, \tag{4.1}$$

where I is the input into the system. If I is strictly positive, then equation 4.1 "blows up" in a finite amount of time. This suggests a nonlinear integrate-and-fire model in which x is reset to $-\infty$ when it grows to ∞. Blowing up to infinity is equivalent to eliciting a spike. Suppose the system is reset to $-\infty$ at $t = 0$. Then for $T > 0$, it will blow up to $+\infty$ at $t = \pi/\sqrt{I}$. Thus, one can think of this as a repetitively firing neuron with a period $\pi/\sqrt{I}$.

This argument can be made formal (see Ermentrout & Kopell, 1986, or Izhikevich, 1999). Equation 4.1 can be changed into a differential equation on the circle by making the transformation $x = \tan(\theta/2)$, whence it becomes the "theta model":

$$\theta' = 1 - \cos\theta + (1 + \cos\theta)I. \tag{4.2}$$

Firing occurs when $\theta(t) = \pi$. Since we are interested in the oscillatory case, the parameter I can be set to 1 without loss of generality so that the un-

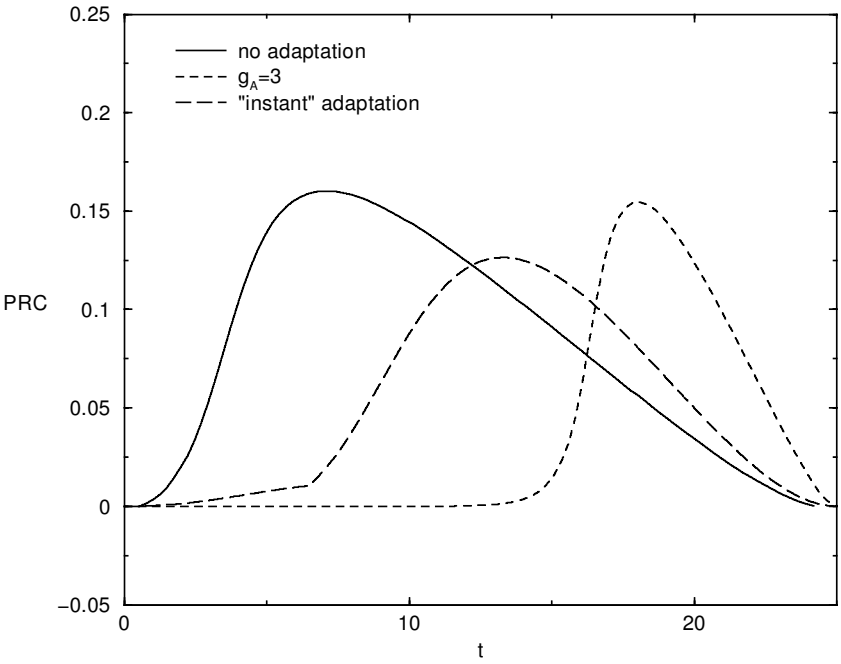

Figure 9: PRC for the theta model with and without adaptation. "Instant" adaptation means the adaptation modeled as a fixed delay of about a third of the period with amplitude 3.

coupled theta model satisfies $\theta' = 2$. Thus, $\theta(t) = 2t + \theta(0)$. The model fires when x in equation 4.1 goes to infinity or when $\theta = \pi$ in equation 4.2. The PRC for this simple model is obtained by instantly incrementing x in equation 4.1 by an amount g.

In the appendix, we derive the PRC for this model and obtain

$$P(t; g) = \frac{1}{2} + \frac{1}{\pi} \arctan(\tan(t - \pi/2) + g) - t/\pi. \tag{4.3}$$

Thus, for instantaneous perturbations, the PRC of the theta model is explicitly computable and is shown in Figure 9. It is strictly positive and for small g is approximately proportional to $1 - \cos 2t$.

We next ask how adaptation affects the PRC of the theta model. Izhikevich (2000) shows that if you add adaptation with slow decay, then the theta model becomes:

$$\theta' = (1 - \cos\theta) + (1 + \cos\theta)(I - g_a z) \tag{4.4}$$

$$\tau_a z' = \delta(\theta - \pi) - z. \tag{4.5}$$

The PRC cannot be analytically found for this model. However, we can do exactly the same as one would do in an experiment and compute the PRC by applying a brief pulse at different times. The result of this computation is shown in Figure 9. As with the full biophysical models, the effect of adaptation is to suppress the excitability after the pulse.

To gain some insight into how the adaptation has this suppressive effect at the early part of the PRC, we introduce a simplified version of adaptation that is analytically tractable. We apply a negative delta function perturbation with magnitude g_a to a cell at fixed time τ_a after it has fired. That is, we approximate the exponential adaptation, $g_a \exp(-t/\tau_a)$, by a single pulse concentrated τ_a units later. In this case, we can explicitly compute the PRC (see the appendix). Figure 9 shows the result of the calculation. Several effects are clear: the peak response is delayed considerably, the response shortly after the spike is strongly suppressed, and the slope is increased for inputs that occur right before the spike. These effects conspire to push the two neurons toward synchrony.

To close this section, we consider a pair of theta neurons that have both instantaneous delta function coupling (resetting using the PRC) and delayed negative feedback. Thus, the model consists of a pair of theta neurons with a fixed current bias, $I = 1$, subject to the following rule: Each time $\theta_j = \pi$, it is reset to $\theta_j = -\pi$; oscillator $k \neq j$ is reset to

$$\theta_k = 2 \arctan(\tan(\theta_k/2) + g);$$

and τ_a time units later, θ_j receives a negative impulse of strength, g_a:

$$\theta_j = 2 \arctan(\tan(\theta_j/2) - g_a).$$

(The derivation of these resetting functions is in the appendix.) The usefulness of this simple model is that it can be directly reduced to a map for the timing differences. That is, we let $T_j(n)$ denote the time of the nth firing of unit j, we assume identical units, and finally, we assume that τ_a is larger than the initial time difference between the two units. This latter assumption simplifies the construction of the map and eliminates multiple cases. Let $\phi_n = T_2(n) - T_1(n)$. The map, $\phi \to M(\phi)$, is the composition of several functions:

$$\begin{aligned}
x_1(\phi) &= \tan(\phi - \pi/2) + g \\
x_2(\phi) &= \tan[-\phi + \tau_a + \arctan x_1(\phi)] - g_a \\
T_p(\phi) &= \pi/2 - \arctan(x_2(\phi)) + \tau_a \\
y_2(\phi) &= \tan[T_p(\phi) - \phi - \tau_a - \arctan(\cot \tau_a + g_a)] + g \\
\phi_{n+1} &= \pi/2 - \arctan(y_2(\phi)) \equiv M(\phi).
\end{aligned}$$

The derivation is in the appendix. First, note that by direct substitution, one finds that $\phi = 0$ is a fixed point. Next suppose that there is no adaptation,

so that $g_a = 0$. Then the map simplifies to

$$\phi_{n+1} = \phi_n,$$

no matter what the coupling strength. That is, in the absence of adaptation, the map is degenerate and has no effect on the timing differences. We can expand the map with adaptation ($g_a > 0$) around the synchronous fixed point to study its local dynamics. Using Maple V, we expand the map in a power series in ϕ and find that to cubic order:

$$M(\phi) = \phi - g_a g^2 \frac{g_a + 2\cot\tau_a}{1 + (g_a + \cot\tau_a)^2}\phi^3 \equiv \phi - C\phi^3.$$

Because the adaptation and synapses are instantaneous, the linearized map is degenerate. However, the adaptation adds a nonlinear effect to the origin. Since the coefficient of the cubic term is negative, this implies that the origin is an attracting fixed point. It is crucial that the adaptation delay, τ_a, be positive since otherwise the limiting coefficient of ϕ^3 will be zero and the origin will again be neutrally stable.

This map provides some additional insight. We expect that if the synapses and the adaptation are not instantaneous, then the linear coefficient will not be identically 1. Suppose that we introduce a small parameter, μ, that represents the effects of finite (but nonzero) synaptic and adaptation persistence. Then the map is approximately given by

$$\phi_{n+1} = (1 + \mu)\phi_n - C\phi_n^3.$$

If $\mu < 0$, then the origin is stable, and we obtain stable synchrony to the perturbed map. However, if $\mu > 0$, then the origin is unstable, and synchrony is not a stable solution. However, since $C > 0$, for $\mu > 0$, there is a pair of stable fixed points: $\bar{\phi} = \pm\sqrt{\mu/C}$. That is, we find a nearly synchronous timing difference between the two units identical in local behavior to the last panels in Figures 6B and 7D. Numerical simulations of a pair of theta models using instant adaptation and synapses whose dynamics are not instantaneous show that synchrony is unstable. Instead, the pair tends to a nearly synchronous solution with a phase difference that tends to zero as the synapses speed up. Figure 10 shows the phase difference between the two oscillators for synapses that have the form $s(t) = b\exp(-bt)$ as a function of the parameter b. As $b \to \infty$, $s(t)$ approaches a delta function, and ϕ appears to approach the synchronous solution. The approach seems to follow a power law that is consistent with the fact that for infinitely fast synapses, the synchronous solution is stable but not exponentially stable.

5 Conclusions

We have shown that the addition of adaptation to a spiking Class 1 neural model has effects on the ability of the neuron to synchronize with other

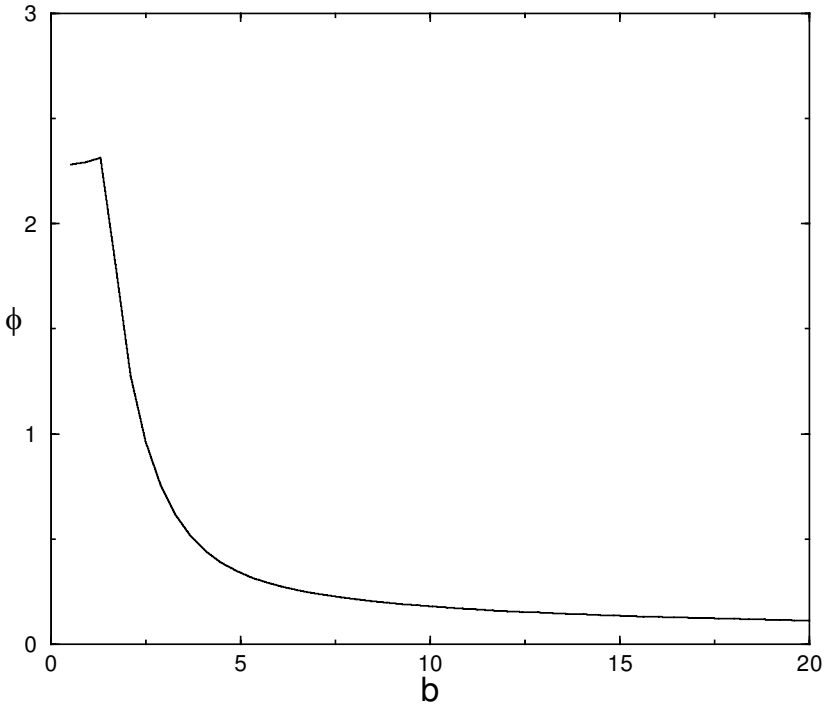

Figure 10: Phase difference between two theta models with delayed instant adaptation and time-dependent exponential synapses, $s(t) = b\exp(-bt)$. As $b \to \infty$ the phase difference tends to zero.

cells. This was shown to be a consequence of the effects of the adaptation on the PRC. For M current–based adaptation, the current has a global effect on the bifurcation diagram through a destabilization of the rest state at high enough currents. This leads to a PRC that is negative for a short time after the spike.

Intuitively, what is going on is that right after the spike, the adaptation-related potassium gates are not fully saturated, and the additional depolarizing currents from an excitatory synapse open them further. This delays the onset of the next spike. The calcium-based adaptation acts more like a shunt since it is already close to saturation due to its sharpness of onset. The recurrent inhibition acts in a way similar to the calcium-based adaptation. Thus, the synaptic depolarization occurring after a spike is largely ignored. The effects are more subtle since the phase cannot be delayed due to an excitatory stimulus. Thus, intuition fails (or is, at least, not obvious), and detailed calculations are necessary.

van Vreeswijk and Hansel (in press) have recently explored the effects of adaptation in integrate-and-fire models. They have sufficiently strong recurrent excitatory coupling such that with adaptation, the result of connecting two neurons together is bursting. This is a different regime from that studied here. The adaptation in their models builds up slowly and is strong enough to shut the neurons off. After the neurons recover from the adaptation, they fire again. The recurrent excitation leads to rapid firing. Thus, the adaptation leads to a pattern of bursts that are synchronized. However, the spikes within the burst are not synchronized. In this article, the synapses are not sufficiently strong to induce bursting.

Adaptation and negative feedback have a dramatic effect on the firing rate versus current curve of cortical neurons (Ermentrout, 1998). The computations and analysis in this article show that they also have a big effect on the synchronization properties of excitatorily coupled neurons. More generally, the presence of a delayed negative feedback makes it possible to synchronize or nearly synchronize two excitatorily coupled cells that would not synchronize without the feedback.

Appendix

Here, we present the equations used in the article. The general equations for all neurons have the form:

$$
\begin{aligned}
Cv' &= I - g_{na}hm^3(v - e_{na}) - \left(g_k n^4 + g_m w + g_{ahp}\frac{ca}{ca+1}\right)(v - e_k) \\
&\quad - g_l(v - e_l) - i_{ca} \\
m' &= a_m(v)(1 - m) - b_m(v)m \\
n' &= a_n(v)(1 - n) - b_n(v)n \\
h' &= a_h(v)(1 - h) - b_h(v)h \\
w' &= (w_\infty(v) - w)/t_w(v) \\
ca' &= -0.002 i_{ca} - ca/80 \\
i_{ca} &= g_{ca} m_{l,\infty}(v)(v - e_{ca}) \\
m_{l,\infty}(v) &= 1/(1 + \exp(-(v + 25))/2.5)) \\
a_m(v) &= 0.32(54 + v)/(1 - \exp(-(v + 54)/4)) \\
b_m(v) &= 0.28(v + 27)/(\exp((v + 27)/5) - 1) \\
a_h(v) &= 0.128\exp(-(50 + v)/18) \\
b_h(v) &= 4/(1 + \exp(-(v + 27)/5)) \\
a_n(v) &= 0.032(v + 52)/(1 - \exp(-(v + 52)/5)) \\
b_n(v) &= 0.5\exp(-(57 + v)/40) \\
t_w(v) &= 100/(3.3\exp((v + 35)/20.0) + \exp(-(v + 35)/20.0)) \\
w_\infty(v) &= 1.0/(1.0 + \exp(-(v + 35)/10.0)).
\end{aligned}
$$

Synaptic gates satisfy

$$s' = \alpha(1 - s)/(1 + \exp(-(v + 10)/10)) - \beta s. \tag{A.1}$$

Units are mS/cm^2 for the conductances, milliseconds for time, millivolts for voltage, μF/cm^2 for capacitance, and μA/cm^2 for currents.

The parameters are $e_k = -100, e_{na} = 50, e_l = -67, e_{ca} = 120$, $g_l = 0.2, g_k = 80, g_{na} = 100, c = 1$, $g_{ca} = 1$, $\alpha = 2$, $\beta = 0.1$. The parameters g_m, g_{ahp}, and I varied from simulation to simulation depending on whether the adaptation was on. Typically, g_m, g_{ahp} were on the order of 1–2.

Simulations with inhibitory neurons consisted of a single excitatory (E) and inhibitory (I) pair (cf. Figures 3 and 7). I cells have the same intrinsic dynamics as the E cells but lack any adaptation currents. The E cells receive a bias current $I = 3.5$, and the I cells receive no bias current. Connection strengths are $g_{e\to i} = 0.1$ and $g_{i\to e} = 1$. E synapses obey equation A.1 with $\alpha = 10$ and $\beta = 5$, while for the inhibitory synapses, $\alpha = 2$ and $\beta = 0.1$. Synaptic reversal potentials were 0 for the excitatory synapses and -80 for the inhibitory synapses. These small subnetworks (of one E and one I cell) are coupled together through excitatory-excitatory interactions with $g_{e\to e} = 0.01$ for Figure 3.

A.1 The Canonical Maps. Here we derive all of the maps and PRCs for the theta model with instantaneous adaptation and synapses. It is more convenient to work with the untransformed equations,

$$\frac{dx}{dt} = x^2 + 1, \tag{A.2}$$

where we have assumed without loss in generality that the applied current, $I = 1$. This is an integrate-and-fire model, but firing occurs when x goes to infinity and the reset is $x = -\infty$. The quadratic nonlinearity enables the system to blow up in a finite amount of time. The solution to equation A.2 for $x(0) = a$ is

$$x(t) = \tan(t + \arctan(a)).$$

This calculation shows that the next "spike" occurs (i.e., x goes to infinity) at

$$T_f(a) = \pi/2 - \arctan(a). \tag{A.3}$$

If $x(0) = -\infty$, then $x(t) = \infty$ when $t = \pi$. Thus, the period of the unperturbed system is π. Now suppose that at $t = 0$, x is reset to $-\infty$, and at $t = s < \pi$ a delta function pulse of strength g is applied. Then right after the pulse,

$$x(s^+) = x(s^-) + g = \tan(s - \pi/2) + g.$$

Thus, from equation A.3, the time of firing is now

$$\hat{T}(s) = s + \pi/2 - \arctan(\tan(s - \pi/2) + g),$$

from which we deduce the PRC:

$$\Delta(t) = \frac{\pi - \hat{T}(t)}{\pi} = \frac{1}{2} + \frac{1}{\pi}\arctan(\tan(t - \pi/2) + g) - \frac{t}{\pi}. \tag{A.4}$$

As a by-product of this calculation, we can obtain the phase-resetting curve for the theta model. That is, given that $\theta = \theta_0$ when the impulse comes in, what is the new value of θ? Since $\theta(t) = -\pi + 2t$, we see that $t = \pi/2 + \theta/2$. Thus, in terms of θ, the value of x after an impulse is

$$x = \tan(\theta/2) + g,$$

and thus

$$\theta_{new} = 2\arctan(\tan(\theta_{old}/2) + g). \tag{A.5}$$

Next, suppose that we add the delayed adaptation with strength g_a and delay τ_a. First, we compute the unperturbed period. At $t = \tau_a^+$,

$$x(\tau_a) = \tan(\tau_a - \pi/2) - g_a,$$

so that the period of the oscillation is

$$T_a = \tau_a + \pi/2 - \arctan(\tan(\tau_a - \pi/2) - g_a).$$

Note that if $g_a = 0$ or $\tau_a = 0$, then $T_a = \pi$, the unperturbed period. We compute the PRC for this model assuming a pulse arises at a time t after firing. Suppose that $t < \tau_a$. Then

$$x(t) = \tan(t - \pi/2) + g \equiv x_1.$$

We next compute the value of x when the delayed adaptation kicks in, x_2:

$$x_2 = \tan(\tau_a - t + \arctan(x_1)) - g_a.$$

The time of firing is then

$$\hat{T} = T_f(x_2) + \tau_a.$$

This gives us the PRC for perturbations that arise before $t = \tau_a$. Similar calculations are done for the case in which the perturbation occurs after the

adaptation occurs. These two cases together allow us to derive the function for the PRC with the adaptation that is shown in Figure 9.

Finally, we derive the map for two theta models with instant adaptation and instant synapses. We will suppose for simplicity that the timing difference between them is less than the adaptation time. The following events occur. Cell 1 fires, cell 2 fires, cell 1 receives adaptation, cell 2 receives adaptation, cell 1 fires, and cell 2 fires, completing the cycle. Cell 1 fires at $t = 0$ and cell 2 at $t = \phi$. Thus, cell 1 receives synaptic input and has the value

$$x_1(\phi) = \tan(\phi - \pi/2) + g.$$

The next thing to occur is the adaptation of cell 1, which occurs at a time τ_a, leaving cell 1 with the value

$$x_2(\phi) = \tan(\tau_a - \phi + \arctan(x_1)) - g_a.$$

At $t = \phi + \tau_a$, cell 2 receives adaptation so that its value is

$$y_1 = \tan(\tau_a - \pi/2) - g_a = -(g_a + \cot \tau_a).$$

Next cell 1 fires at

$$T_1(\phi) = \pi/2 - \arctan(x_2(\phi)) + \tau_a,$$

which induces a phase shift on cell 2:

$$y_2(\phi) = \tan[T_1(\phi) - \phi - \tau_a + \arctan y_1] + g.$$

Finally cell 2 fires at

$$T_2 = T_1 + \pi/2 - \arctan y_2(\phi).$$

Thus the new timing difference is

$$\phi' = T_2 - T_1 = \pi/2 - \arctan y_2(\phi) \equiv M(\phi).$$

Thus, the map M is the composition of several readily computable maps.

Acknowledgments

The research reported in this article was supported by the National Institute of Mental Health and the National Science Foundation. We thank Alex Reyes for kindly providing the data for Figure 8.

References

Connor, J. A., Walter, D., & McKown, R. (1977). Neural repetitive firing: Modification of the Hodgkin-Huxley axon suggested by experimental results from crustacean axons. *Biophys. J., 18*, 81–102.

Crook, S. M., Ermentrout, G. B., & Bower, J. M. (1998). Spike frequency adaptation affects the synchronization properties of networks of cortical oscillations. *Neural Comput., 10*, 837–854.

Ermentrout, B. (1996). Type I membranes, phase resetting curves, and synchrony. *Neural Comput., 8*, 979–1001.

Ermentrout, B. (1998). Linearization of F-I curves by adaptation. *Neural Comput., 10*, 1721–1729.

Ermentrout, G. B., & Kopell, N. K. (1984). Frequency plateaus in a chain of weakly coupled oscillators I. *SIAM J. Math. Analysis, 15*, 215–237.

Ermentrout, G. B., & Kopell, N. (1986). Parabolic bursting in an excitable system coupled with a slow oscillation. *SIAM J. Appl. Math., 46*, 233–253.

Ermentrout, G. B., & Kopell, N. K. (1991). Multiple pulse interactions and averaging in systems of coupled neural oscillators. *J. Math. Biology, 29*, 195–217.

Ermentrout, G. B., & Kopell, N. K. (1998). Fine structure of neural spiking and synchronization in the presence of conduction delays. *Proc. Natl. Acad. Sci., 95*, 1259–1264.

Gray, C. M., Engel, A. K., Konig, P., & Singer, W. (1992). Synchronization of oscillatory neuronal responses in cat striate cortex: Temporal properties. *Vis. Neurosci., 8*, 337–347.

Hansel, D., Mato, G., & Meunier, C. (1995). Synchrony in excitatory neural networks. *Neural Comput., 7*, 307–337.

Hoppensteadt, F., & Izhikevich, E. (1997). *Weakly connected neural nets*. Berlin: Springer-Verlag.

Izhikevich, E. M. (1999). Class 1 neural excitability, conventional synapses, weakly connected networks, and mathematical foundations of pulse-coupled models. *IEEE Trans. Neur. Networks, 10*, 499–507.

Izhikevich, E. M. (2000). Neural excitability, spiking, and bursting. *International Journal of Bifurcation, 10*, 1171–1267.

Kopell, N., Ermentrout, G. B., Whittington, M. A., & Traub, R. D. (2000). Gamma rhythms and beta rhythms have different synchronization properties. *Proc. Natl. Acad. Sci. USA, 97*, 1807–1872.

Kuramoto, Y. (1982). *Chemical oscillations, waves, and turbulence*. New York: Springer-Verlag.

McCormick, D. A., Connors, B. W., Lighthall, J. W., & Prince, D. A. (1985). Comparative electrophysiology of pyramidal and sparsely spiny stellate neurons in the neocortex. *J. Neurophysiol., 54*, 782–806.

Morris, C., & Lecar, H. (1981). Voltage oscillations in the barnacle giant muscle fiber. *Biophy J., 35*, 193–213.

Reyes, A. D., & Fetz, E. E. (1993a). Effects of transient depolarizing potentials on the firing rate of cat neocortical neurons. *J. Neurophysiol., 69*,1673–1683.

Reyes, A. D., & Fetz, E. E. (1993b). Two modes of interspike interval shortening by brief transient depolarizations in cat neocortical neurons. *J. Neurophysiol., 69*, 1661–1672.

Rinzel, J. M., & Ermentrout, G. B. (1998). Analysis of neuronal excitability. In C. Koch and I. Segev (Eds.), *Methods in neuronal modeling* (2nd ed.). Cambridge, MA: MIT Press.

Traub, R. D., Jefferys, J. G. R., & Whittington, M. A. (1999). *Fast oscillations in cortical circuits*. Cambridge, MA: MIT Press.

Traub, R. D., & Miles, R. (1991). *Neuronal networks of the hippocampus*. New York: Cambridge University Press.

van Vreeswijk, C., Abbott, L. F., & Ermentrout, G. B. (1994). When inhibition not excitation synchronizes neural firing. *J. Comput. Neurosci., 1*, 313–321.

van Vreeswijk, C., & Hansel, D. (in press). Patterns of synchrony in neural networks with spike adaptation. *Neural Computation*.

Wang, X. J. (1998). Calcium coding and adaptive temporal computation in cortical pyramidal neurons. *J. Neurophys., 79*, 1549–1566.

Williams, T. L., & Bowtell, G. (1997). The calculation of frequency-shift functions for chains of coupled oscillators, with application to a network model of the lamprey locomotor pattern generator. *J. Comput. Neurosci., 4*, 47–55.

Received January 25, 2000; accepted August 1, 2000.